Progress In Electromagnetics Research B, Vol. 43, 239–253, 2012

ELECTROMAGNETIC ANALYSIS OF A MODULAR FLUX-SWITCHING PERMANENT-MAGNET MOTOR USING FINITE-ELEMENT METHOD

W. Zhao[1, *], M. Cheng[2], J. Ji[1], and R. Cao[2]

[1]School of Electrical and Information Engineering, Jiangsu University, No. 301 Xuefu Road, Zhenjiang, China

[2]School of Electrical Engineering, Southeast University, No. 2 Si-pai-lou, Nanjing, China

Abstract—This paper proposes a new 3-phase flux-switching permanent-magnet (FSPM) motor termed as modular FSPM (M-FSPM) motor, for high reliability applications. Due to PMs in the stator, the proposed motor offers high efficiency, simple and robust rotor structure, and good thermal dissipation conditions. The key is the new motor topology which incorporates the concept of fault-tolerant teeth to provide the desired decoupling among phases. By using finite element method, the proposed M-FSPM motor is analyzed as compared with the existing fault-tolerant FSPM (FT-FSPM) motor. The results show that the proposed M-FSPM motor not only retains the merits of high power density, strong mechanical integrity, good immunity from thermal problem and high torque capability, but also offers lower torque ripple, higher average torque and lower cost than the existing FT-FSPM motor. A proposed M-FSPM motor is designed and built for exemplification. Experimental results of the prototype are given to confirm the validity of the proposed motor.

1. INTRODUCTION

High reliability is an essential requirement for critical applications, where any types of fault would lead to disastrous effects on safety and system performance. Continual operation of motor drives has been a growing demand and fault-tolerant drive systems that are cost effective without sacrificing their post-fault performance are therefore desirable for automotive, aerospace and military applications [1, 2].

Received 29 June 2012, Accepted 23 August 2012, Scheduled 1 September 2012

* Corresponding author: Wenxiang Zhao (zwx@ujs.edu.cn).

In recent years, the development of fault-tolerant motor drives has received a great attention, focusing on the switched reluctance (SR) motor and the conventional permanent-magnet (PM) brushless motor. SR motors have simple rotor construction and mechanical robustness [3, 4]. Moreover, due to their decoupling magnetic and circuit phases, SR motors inherently possess fault-tolerant characteristic. Ref. [5] discussed issues that are pertinent to the fault classification in a SR motor drive. Then, some remedial operations were adopted in order to improve fault-tolerant performance of SR motor drives. Ref. [6] proposed a new multi-phase SR motor drive with outer-rotor topology for high reliability traction applications, in which an integrated inverter was adopted to increase the number of motor phases without increasing the number terminals. On the other hand, PM motors are emerging as a promising candidate for high power density and high efficiency applications compared with SR motors [7]. A number of PM motors and control strategies with differing degrees of fault-tolerant capability have appeared in the literature [8]. By employing an arrangement of alternately wound teeth in the stator, a fractional-slot concentrated-windings PM motor, termed as fault-tolerant rotor-PM motor, was proposed for high reliability operation [9]. To operate the fault-tolerant rotor-PM motor at flux weakening mode, a new control strategy was proposed in [10]. In addition, multi-phase PM motors have received many attentions for fault-tolerant operation. In [11], a postfault current control strategy of a 5-phase PM motor was proposed. The proposed control strategy guarantees safe drive operation considering the 3-rd harmonic components of back-EMF.

However, since PMs are located in the rotor, the conventional PM brushless motors suffer from weak mechanical structure and difficulty of PM cooling. Hence, how to incorporate the merits of both high reliability and high efficiency has attracted more and more attentions. To retain the advantages of both SR and rotor-PM motors, a new class of brushless motors having PMs in the stator (stator-PM motor), including the doubly-salient PM (DSPM), flux-reversal PM (FRPM) and flux-switching PM (FSPM) types, have been introduced [12]. Extensive research work has been performed to evaluate this class motors, showing that stator-PM motors incorporate the merits of high power density, robust structure, and free from thermal problem on PMs [13–15]. Recent research has identified that the DSPM motor can inherently offer fault-tolerance [16]. However, it has been identified that the FSPM motor has significantly higher torque capability than the DSPM one [17]. For the purpose of introducing fault-tolerant concept into the FSPM motor, a new FSPM motor with redundant

structure, termed as R-FSPM motor, has been proposed [18, 19]. However, it should be noted that R-FSPM motors suffer from the magnetic coupling between phases, which decreases the fault-tolerant performance of motor. Recently, new fault-tolerant FSPM (FT-FSPM) motor topologies, in which each phase is magnetically and physically isolated, have been proposed. In [20], a flux barrier is set in a linear FSPM motor topology, whereas fault-tolerant capability was enhanced but the power density was decreased. By employing an arrangement of alternately wound teeth in the stator, a new FT-FSPM motor has also been proposed [21]. Although this FT-FSPM motor can offer high torque capability with fault-tolerance, it suffers from severe asymmetry in flux linkage and hence back-EMF waveforms, thus causing serious torque ripples. Even with the use of rotor skewing to enhance more sinusoidal back-EMF waveforms at the cost of reducing the voltage amplitude, the problem of asymmetry cannot be solved.

The purpose of this paper is to propose a new FSPM motor, termed as modular FSPM (M-FSPM) motor, which can not only retain the advantages of the FSPM motor, but also solve the problems of the existing FT-FSPM motor. In Section 2, the topology and the operation principle of the proposed motor will be presented. Section 3 will be devoted to analyze the electromagnetic characteristics by using finite element method (FEM), in which a quantitative comparison between the proposed M-FSPM and the existing FT-FSPM motors will be performed. In Section 4, the experimental verification will be given. Finally, conclusions will be drawn in Section 5.

2. TOPOLOGY AND OPERATION PRINCIPLE

Figure 1 shows the topology of the proposed 3-phase M-FSPM motor. It can be seen that the proposed motor adopts a modular structure with 24 salient teeth in the stator and 14 salient poles in the rotor. The key of this topology is the introduction of 12 fault-tolerant teeth (FTT) interleaving with 12 armature teeth. Thus, the phase windings of adjacent stator poles are essentially isolated, leading to the merit of phase decoupling. This merit is highly desirable to enable fault-tolerant operation. Namely, when there is a fault in one of the phase windings, the remaining healthy phase windings can continually operate with reasonable performance.

Different from the conventional FSPM motor in which the stator is constructed from a number of U-shaped laminated segments, the proposed M-FSPM motor adopts the E-shaped laminated segments to build the stator. Namely, twelve pieces of PMs are placed in between these E-shaped laminated segments, and provide the desired

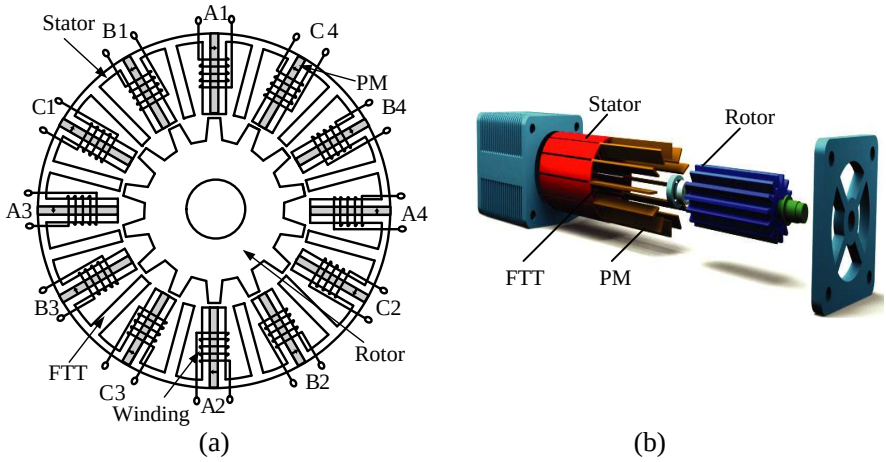

Figure 1. Proposed M-FSPM motor. (a) Cross-section. (b) Configuration.

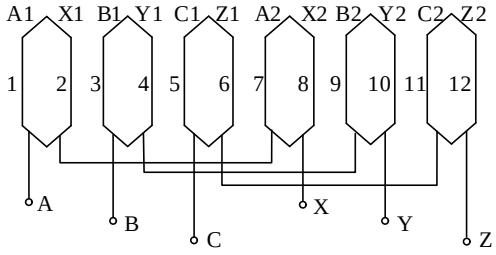

Figure 2. Armature winding connection.

field excitation. The armature windings on the diametrically opposite stator poles are connected in series to form one phase winding, as shown in Figure 2.

Since there are no PMs, brushes, nor windings in the rotor, the proposed motor provides the advantages of simple rotor configuration and mechanical robustness. Also, since all PMs are located in the stator, the problem of cooling difficulty and thermal instability can be eliminated. Therefore, the proposed M-FSPM motor inherits the merits of stator-PM motors while providing the capability of fault tolerance.

Figure 3 illustrates the operation principle of the M-FSPM motor. It can be known that the fluxes produced by PMs always go through the magnetic path where the reluctance is minimal, i.e., the positions

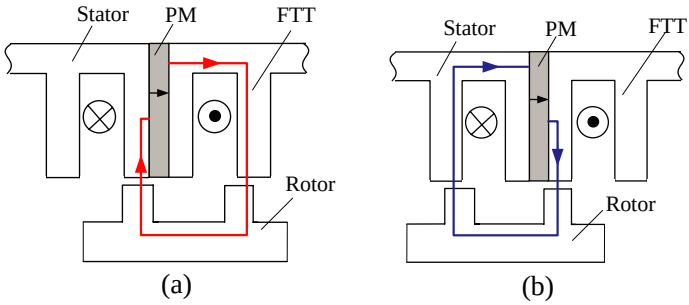

Figure 3. Operation principle of M-FSPM motor. (a) First position. (b) Second position.

where the rotor poles align with the stator teeth. Hence, at the first position as shown in Figure 2(a), the rotor pole aligns with one of two stator teeth over which a coil is wound and the PM flux linked in the coil goes out of the stator and into the rotor pole. When the rotor moves forward to the second position as shown in Figure 2(b), the PM flux goes out of the rotor pole and into the stator tooth, realizing "flux-switching", from which the operating principle of flux-switching of this motor is named. Therefore, as the rotor moves, the flux linkage in the windings will change periodically.

3. ELECTROMAGNETIC PERFORMANCE

3.1. Finite Element Method

In this section, FEM is adopted to analyze electromagnetic performance of the proposed M-FSPM motor [22–24].

Firstly, the electromagnetic field equation of the motor is governed by

$$\begin{cases} \Omega : \frac{\partial}{\partial x}\left(\upsilon\frac{\partial A}{\partial x}\right) + \frac{\partial}{\partial y}\left(\upsilon\frac{\partial A}{\partial y}\right) = -J - \upsilon\left(\frac{\partial B_{ry}}{\partial x} - \frac{\partial B_{rx}}{\partial y}\right) + \sigma\frac{\partial A}{\partial t} \\ S_1 : A = 0 \end{cases} \quad (1)$$

where Ω is the region of calculation, A the magnetic vector potential component along the z axis, J the current density, υ the reluctivity, and σ the electrical conductivity. B_{rx} and B_{ry} are, respectively, the remnant flux density components of the PM along the x and y axes, and S_1 is the boundary of the region of calculation.

Secondly, the armature circuit equation of the motor is expressed

as:

$$(R_s + R_r)i + (L_s + L_r)\frac{di}{dt} = \frac{l}{s}\iint_{\Omega}\frac{\partial A}{\partial t}d\Omega \tag{2}$$

where i is the phase current, and R_s and L_s are the winding resistance and inductance, respectively, R_r and L_r are the load resistance and inductance, respectively. S is the sectional area of the conductor of each phase, and l is the axial length of iron core.

Thirdly, the motion equation is given by

$$T_e - T_l - B\omega = J_m\frac{d\omega}{dt} \tag{3}$$

where J_m is the moment of inertia, ω the rotor speed, B the damping coefficient, T_e the electromagnetic torque, and T_l the load torque.

Finally, after coupling (1) to (3) and applying discretization, the FEM can be performed to calculate magnetic field of the motor.

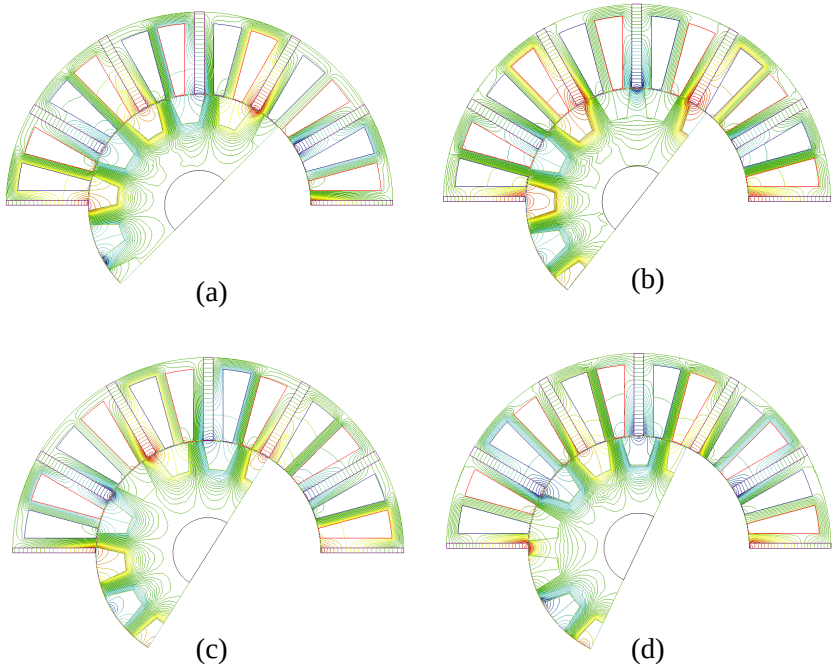

Figure 4. Open-circuit magnetic field distributions at four typical rotor positions. (a) $\theta_r = 0°$. (b) $\theta_r = 90°$. (c) $\theta_r = 180°$. (d) $\theta_r = 270°$.

3.2. Analysis

Figure 4 shows the open-circuit magnetic field distributions of the proposed M-FSPM motor at different rotor positions. It can be seen that both the magnitudes and polarities of the PM fluxes linked in the coil windings will change periodically when the rotor is at the four typical positions.

Figure 5 compares the magnetic field distributions due to the PMs only and the armature current only, respectively. Since the windings and the PMs are magnetically in parallel, rather than in series as in most rotor-PM motors, the influence of armature reaction field on the working point of PMs under the short-circuit fault is almost eliminated. Thus, this motor is inherently suitable for fault-tolerant operation. Hence, the M-FSPM motor combines the advantages of SR motors (high speed and robust rotor structure), brushless PM motors (high efficiency) and fault-tolerant motors (independent phases). Also, it can be observed from Figure 5(b) that the proposed motor can offer the nature of phase decoupling, namely the magnetic fields of two adjacent phases are independent from one another. Hence, the corresponding self inductances and mutual inductances are calculated. Table 1 lists its inductances as compared with those of the conventional FSPM motor. It can be found that the ratio of mutual inductance to self inductance of the conventional FSPM motor is much larger than that of the proposed M-FSPM motor, indicating that the conventional one exhibits closely coupled phases while the M-FSPM motor are essentially phase decoupling.

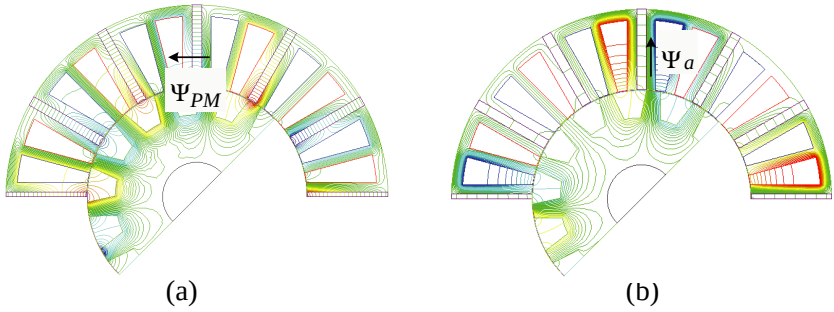

Figure 5. Magnetic field distributions. (a) PMs only. (b) Armature current only.

Table 1. Comparison of self and mutual inductances.

	L (mH)	M (mH)	M/L (%)
Conventional FSPM motor	1.948	0.930	47.7
Proposed M-FSPM motor	4.298	0.550	12.8

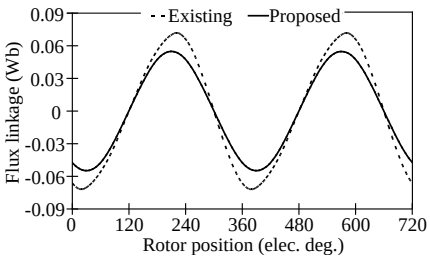

Figure 6. Comparison of flux linkage waveforms.

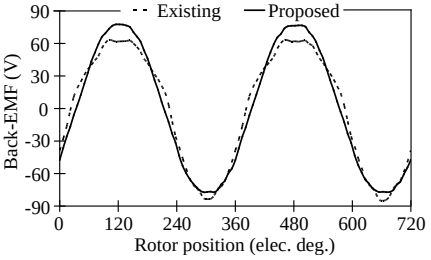

Figure 7. Comparison of back-EMF waveforms.

3.3. Comparison

In order to evaluate the proposed M-FSPM motor as compared with the existing FT-FSPM motor in [21], they are designed based on the same number of phases, rated speed, stator outside diameter, axial length, slot packing factor, total motor volume and total motor mass. Also, both motors adopt the unskewed rotor so that the harmonic distortion or cogging torque will not be unduly influenced. Table 2 lists their design parameters in such a way that they produce the same peak-to-peak value of back-EMFs. It can be found that the proposed motor requires about 61% PMs and 121% copper windings of the existing one. Since PM material is much more costly than copper, the proposed motor takes the definite advantage of lower cost.

Firstly, Figure 6 shows the open-circuit flux linkage waveforms of the two FSPM motors. It can be seen that the existing motor has a higher peak-to-peak value of flux linkage than the proposed one, but with severe asymmetry. Such higher value of flux linkage is simply due to the use of more PMs, whereas the asymmetry is due to the unbalanced arrangement of phase coils.

Secondly, the corresponding back-EMF waveforms at 1000 rpm are shown in Figure 7. It can be found that both FSPM motors have practically the same peak-to-peak value of back-EMF waveforms. Obviously, the proposed motor has a much more sinusoidal and symmetric back-EMF waveform than the existing one. Namely, the

Table 2. Design parameters of existing and proposed FSPM motors.

	Existing	Proposed
Number of phases	3	3
Rated speed (rpm)	1500	1500
Stator outside diameter (mm)	128	128
Stator inside diameter (mm)	70.4	70.4
Rotor inside diameter (mm)	22	22
Air-gap length (mm)	0.35	0.35
Axial length (mm)	75	75
Slot packing factor	0.4	0.4
Total motor volume (cm^3)	965	965
Total motor mass (kg)	5.7	5.7
Number of stator poles	12	12
Number of rotor poles	10	14
Stator tooth arc (degree)	7.5	4.6
Rotor tooth arc (degree)	10.5	7.0
Magnet remanence (T)	1.2	1.2
Magnet relative permeability	1.05	1.05
Magnet volume (cm^3)	119	72.6
Number of coil turns	140	170
Effective slot area (mm^2)	528	636
Phase resistance (Ω)	0.37	0.44

positive and negative peak values of the back-EMF waveform of the proposed motor are 77 V and −77 V, respectively, whereas those values of the existing one are 62 V and −84 V, respectively.

Thirdly, by applying spectral analysis to the back-EMF waveforms, the corresponding fundamental components and harmonic spectra can be deduced. The fundamental RMS voltage of the existing FT-FSPM motor is 51.9 V while that of the proposed M-FSPM motor is 56.6 V, illustrating that the proposed one can offer about 10% higher back-EMF. Then, the harmonic spectra are normalized by the respective fundamental components as shown in Figure 8. It can be observed that the existing motor exhibits much more serious harmonic distortion than the proposed one. Namely, the 2nd-order harmonic of the existing one is very significant (about 15%), which is actually the major source for the production of torque ripple. In contrast, the

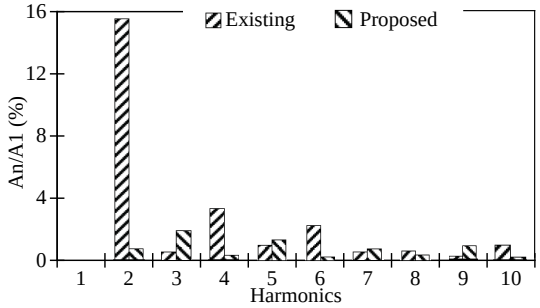

Figure 8. Comparison of back-EMF harmonic spectra.

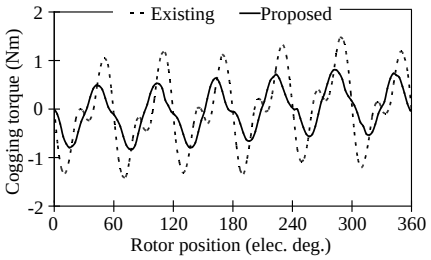

Figure 9. Comparison of cogging torque waveforms.

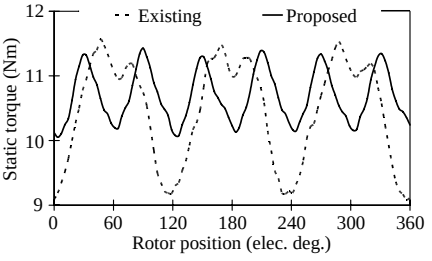

Figure 10. Comparison of static torque waveforms at rated current.

relatively most serious harmonic of the proposed motor is the 3rd-order harmonic, which is actually quite insignificant (about 2%) and does not contribute to the production of torque ripple. Quantitatively, the total harmonic distortion (THD) of the back-EMF waveform of the existing motor is 16.2% which is much higher than the 2.8% of the proposed one.

Fourthly, the cogging torque waveforms of both FSPM motors are simulated as shown in Figure 9. As expected, the proposed motor can offer less pulsating cogging torque than the existing one, which is due to the fact that it requires less PMs and utilizes more teeth. Then, when both motors are fed with sinusoidal currents, so-called the brushless AC (BLAC) mode of operation, the resulting static torque waveforms can be deduced as shown in Figure 10. By defining the torque ripple factor as the percentage ratio of peak-to-peak torque to average torque [18], it can be seen that the torque ripple (12.9%) and average torque (10.7 Nm) of the proposed motor are much better than those (23.9% and 10.4 Nm) of the existing one. It is actually due to the

more sinusoidal and symmetric back-EMF waveform of the proposed M-FSPM motor. Hence, the torque density (average torque per unit mass) of the proposed motor is found to be 1.88 Nm/kg which is larger than the 1.83 Nm/kg of the existing one.

Moreover, in order to evaluate the cost effectiveness of the proposed motor for torque production, the average torque per magnet volume for both FSPM motors is calculated. It confirms that the proposed motor (0.147 Nm/cm^3) is significantly higher than that of the existing one (0.087 Nm/cm^3). Furthermore, the characteristics of average torque and torque ripple versus the peak phase current of both motors are plotted together as shown in Figure 11. It further confirms that the proposed M-FSPM motor can offer higher average torque and much lower torque ripple than the existing FT-FSPM motor.

4. EXPERIMENTAL VERIFICATION

In order to verify the theoretical analysis, a prototype of the M-FSPM motor is designed and built as shown in Figure 12. The measured

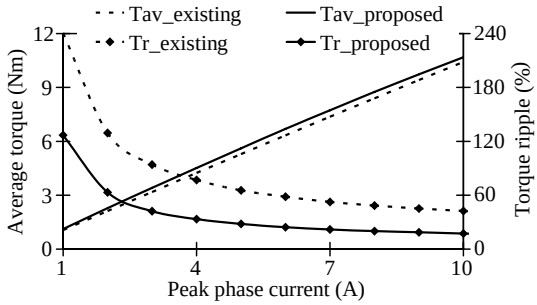

Figure 11. Comparison of average torques and torque ripples.

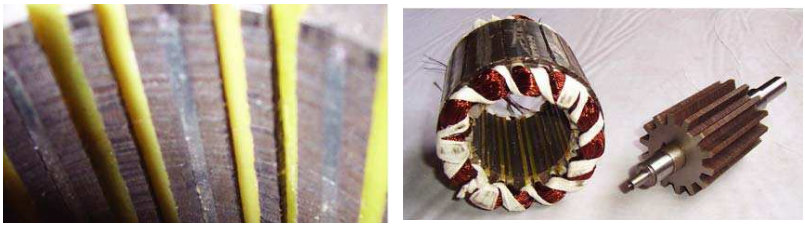

Figure 12. Prototype motor. (a) FTT structure. (b) Stator and rotor.

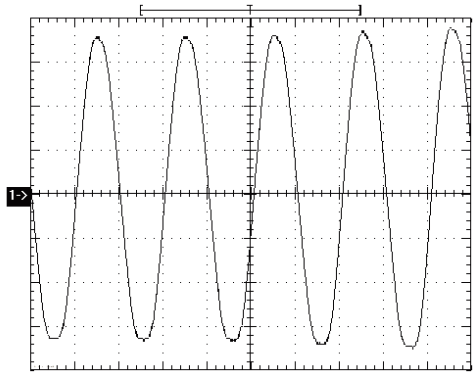

Figure 13. Measured back-EMF waveform (2 ms/div, 20 V/div).

winding back-EMF waveform is shown in Figure 13. As expected, the measured back-EMF waveform closely agrees with the theoretical one shown in Figure 7, verifying the effectiveness of the proposed motor.

5. CONCLUSIONS

A new three-phase M-FSPM motor has been proposed, in which the FTT structure is the key to provide the nature of phase decoupling, and hence the property of fault-tolerance. By using the FEM, the proposed M-FSPM motor has been designed and analyzed. Compared with the existing FT-FSPM motor, it can offer following advantages: first, the required PM material is only 61% of its counterpart for the same peak-to-peak value of back-EMF; second, the back-EMF waveform is much more sinusoidal with the THD lower by 13.4% than that of the existing one; third, the torque ripple is 11% lower than its counterpart; fourth, its cost effectiveness, in terms of the average torque per unit volume of PM material, is 69% higher than the existing one. Both the computer simulation and the experimental results confirm the validity of the proposed M-FSPM motor.

ACKNOWLEDGMENT

This work was supported by the National Natural Science Foundation of China (Projects 60974060 and 51277194), by the Natural Science Foundation of Jiangsu Province (Project SBK201221867) and by the Priority Academic Program Development of Jiangsu Higher Education Institutions.

REFERENCES

1. Chau, K. T. and C. C. Chan, "Emerging energy-efficient technologies for hybrid electric vehicles," *Proceedings of the IEEE*, Vol. 95, No. 4, 821–835, 2007.
2. Cao, W., B. C. Mecrow, G. J. Atkinson, J. W. Bennett, and D. J. Atkinson, "Overview of electric motor technologies used for more electric aircraft (MEA)," *IEEE Transactions on Industrial Electronics*, Vol. 59, No. 9, 3523–3531, 2012.
3. Liang, J., L. Jian, G. Xu, and Z. Shao, "Analysis of electromagnetic behavior in switched reluctance motor for the application of integrated air conditioner on-board charger system," *Progress In Electromagnetics Research*, Vol. 124, 347–364, 2012.
4. Torkaman, H. and E. Afjei, "Comparison of three novel types of two-phase switched reluctance motors using finite element method," *Progress In Electromagnetics Research*, Vol. 125, 151–164, 2012.
5. Gopalakrishnan, S., A. M. Omekanda, and B. Lequesne, "Classification and remediation of electrical faults in the switched reluctance drive," *IEEE Transactions on Industry Applications*, Vol. 42, No. 2, 479–486, 2006.
6. Hennen, M. D., M. Niessen, C. Heyers, H. J. Brauer, and R. W. De Doncker, "Development and control of an integrated and distributed inverter for a fault tolerant five-phase switched reluctance traction drive," *IEEE Transactions on Power Electronics*, Vol. 27, No. 2, 547–554, 2012.
7. Chau, K. T., C. C. Chan, and C. Liu, "Overview of permanent magnet brushless drives for electric and hybrid electric vehicles," *IEEE Transactions on Industrial Electronics*, Vol. 55, No. 6, 2246–2257, 2008.
8. El-Refaie, A. M., "Fault-tolerant permanent magnet machines: A review," *IET Electric Power Applications*, Vol. 5, No. 1, 59–74, 2011.
9. Jack, A. G., B. C. Mecrow, and J. Haylock, "A comparative study of permanent magnet and switched reluctance motors for high-performance fault-tolerant applications," *IEEE Transactions on Industry Applications*, Vol. 32, No. 4, 889–895, 1996.
10. Sun, Z., J. Wang, G. Jewell, and D. Howe, "Enhanced optimal torque control of fault-tolerant permanent magnet machines under flux weakening operations," *IEEE Transactions on Industrial Electronics*, Vol. 57, No. 1, 344–353, 2010.

11. Dwari, S. and L. Parsa, "Fault-tolerant control of five-phase permanent magnet motors with trapezoidal back-EMF," *IEEE Transactions on Industrial Electronics*, Vol. 58, No. 2, 476–485, 2011.
12. Cheng, M., W. Hua, J. Zhang, and W. Zhao, "Overview of stator-permanent magnet brushless machines," *IEEE Transactions on Industrial Electronics*, Vol. 58, No. 11, 5087–5101, 2011.
13. Liu, C., K. T. Chau, J. Z. Jiang, and S. Niu, "Comparison of stator-permanent-magnet brushless machines," *IEEE Transactions on Magnetics*, Vol. 44, No. 11, 4405–4408, 2008.
14. Thomas, A. S., Z. Q. Zhu, and G. W. Jewell, "Comparison of flux switching and surface mounted permanent magnet generators for high-speed applications," *IET Electrical Systems in Transportation*, Vol. 1, No. 3, 111–116, 2011.
15. Zhang, Z., Y. Tao, and Y. Yan, "Investigation of a new topology of hybrid excitation doubly salient brushless DC generator," *IEEE Transactions on Industrial Electronics*, Vol. 59, No. 6, 2550–2556, 2012.
16. Zhao, W., K. T. Chau, M. Cheng, J. Ji, and X. Zhu, "Remedial brushless AC operation of fault-tolerant doubly-salient permanent-magnet motor drives," *IEEE Transactions on Industrial Electronics*, Vol. 57, No. 6, 2134–2141, 2010.
17. Zhu, Z. Q. and J. T. Chen, "Advanced flux-switching permanent magnet brushless machines," *IEEE Transactions on Magnetics*, Vol. 46, No. 6, 1447–1453, 2010.
18. Zhao, W., M. Cheng, W. Hua, H. Jia, and R. Cao, "Back-EMF harmonic analysis and fault-tolerant control of flux-switching permanent-magnet machine with redundancy," *IEEE Transactions on Industrial Electronics*, Vol. 58, No. 5, 1926–1936, 2011.
19. Zhao, W., M. Cheng, R. Cao, and J. Ji, "Experimental comparison of remedial single-channel operations for redundant flux-switching permanent-magnet motor drive," *Progress In Electromagnetics Research*, Vol. 123, 189–204, 2012.
20. Cao, R., M. Cheng, C. Mi, W. Hua, X. Wang, and W. Zhao, "Modeling of a complementary and modular linear flux-switching permanent magnet motor for urban rail transit applications," *IEEE Transactions on Energy Conversion*, Vol. 27, No. 2, 489–497, 2012.
21. Owen, R. L., Z. Q. Zhu, A. S. Thomas, G. W. Jewell, and D. Howe, "Alternate poles wound flux-switching permanent-magnet brushless ac machines," *IEEE Transactions on Industry*

Applications, Vol. 46, No. 2, 790–797, 2010.

22. Torkaman, H. and E. Afjei, "FEM analysis of angular misalignment fault in SRM magnetostatic characteristics," *Progress In Electromagnetics Research*, Vol. 104, 31–48, 2010.
23. Jian, L., G. Xu, G. Yu, J. Song, J. Liang, and M. Chang, "Electromagnetic design and analysis of a novel magnetic-gear-integrated wind power generator using time-stepping finite element method," *Progress In Electromagnetics Research*, Vol. 113, 351–367, 2011.
24. Mahmoudi, A., N. A. Rahim, and W. P. Hew, "Axial-flux permanent-magnet motor design for electric vehicle direct drive using sizing equation and finite element analysis," *Progress In Electromagnetics Research*, Vol. 122, 467–496, 2012.